16th World Conference on Earthquake, 16WCEE 2017

Santiago Chile, January 9th to 13th 2017

Paper N° 0004

Registration Code: S-M1463182058

STRUCTURAL PERFORMANCE OF RECTANGULAR REINFORCED CONCRETE WALLS RETROFITTED BY CARBON FIBER SHEETS

T. Matsui[1], T. Saito[2] , R. Reyna[3]

[1] *Associate Professor, Dept. of Architecture and civil engineering, Toyohashi University of Technology, matsui@ace.tut.ac.jp*
[2] *Professor, Dept. of Architecture and civil engineering, Toyohashi University of Technology, saito@ace.tut.ac.jp*
[3] *PhD. Candidate, Dept. of Architecture and civil engineering, Toyohashi University of Technology, royanyer@gmail.com*

Abstract

Many medium-rise and high-rise reinforced concrete buildings were damaged during the 2010 Maule Chile earthquake. For rectangular reinforced concrete walls that are without boundary column in some buildings, flexural compression failures of multistory shear walls drew a lot of attention. It was found that design of boundary end of structural walls and evaluation of deformation performance of the structural wall was important. On the other hand, it is thought that structural walls of existing buildings which is expected to be flexural compressive failure is preferred to be retrofitted for damage mitigation.

In this study, a performance verification test is conducted on the use of carbon fiber sheets as a retrofitting method for rectangular reinforced concrete shear walls. Note that there have already been several reports published on the effectiveness of carbon fiber sheets retrofitting on walls failing in shear or on walls with a boundary column on one side. The focus is on the retrofitting walls that fail in flexural mode. In other words, although an increase in strength cannot be expected, carbon fiber sheets retrofitting can delay the concrete crushing of the wall base that occurs during flexural failure; and the aim is to verify this improvement in deformation performance due to carbon fiber sheets retrofitting. Three structural wall specimens were prepared in the test. The test variables selected were the presence/absence of carbon fiber sheets retrofitting and the extent of retrofitting. A specimen represents the non-retrofitted test specimen for understanding the basic behavior of the walls. Another specimen was retrofitted over the entire wall span while other specimen was partially retrofitted at the boundary ends of the wall. Specimens were loaded a cyclic horizontal lateral force under a constant axial load. And an additional moment was applied at the top of the specimen by controlling two vertical jacks to correspond to the acting shear force, such that the shear span ratio was 1.5.

From the test, by retrofitting the rectangular reinforced concrete wall with carbon fiber sheets, it was found that post-maximum strength deterioration was more gradual, and deformation performance was improved. And ultimate deformation of specimen which was partially retrofitted at the boundary ends of the wall was larger than that of specimen which was retrofitted over the entire wall span. Strain of concrete of wall base in compression of retrofitted specimen was larger than that of non-retrofitted specimen at the ultimate deformation. Thus, it was expected that concrete of wall retrofitted by carbon fiber sheets would be resistant to lager compressive force than that of non-retrofitted wall in even large strain region. In addition, evaluation of ultimate flexural deformation of specimens was considered based on test results. It was found that calculated ultimate flexural deformation could be good agreement with test results in case of use of plastic hinge lengths of 200mm,which is 2.5 times as long as thickness of wall.

Keywords: Rectangular reinforced concrete wall, Seismic retrofitting, Carbon fiber sheet, ultimate deformation

1. Introduction

Many medium-rise and high-rise reinforced concrete (RC) buildings were damaged during the 2010 Maule Chile earthquake [1]. In particular, for rectangular RC walls that are without boundary column in some buildings, flexural compression failures of multistory walls drew a lot of attention. It was found that design of boundary end of structural walls and evaluation of deformation performance of the structural wall was important. On the other hand, it is thought that structural wall of existing buildings which is expected to be flexural compressive failure is preferred to be retrofitted for damage mitigation.

Authors were conducted a performance verification test on the use of carbon fiber sheets (CFS) as a retrofitting method for rectangular RC structural walls [2]. Note that there have already been several reports published on the effectiveness of carbon fiber sheets retrofitting on walls failing in shear or on walls with a boundary column on one side [3]. The focus is on the retrofitting walls that fail in flexural mode. In other words, although an increase in strength cannot be expected, carbon fiber sheets retrofitting can delay the concrete crushing of the wall base that occurs during flexural failure; and the aim is to verify this improvement in deformation performance due to carbon fiber sheets retrofitting. From the test, by retrofitting the RC wall without boundary columns with CFS, it was found that post-maximum strength deterioration was more gradual, and deformation performance was improved.

In this study, static loading test of rectangular RC walls retrofitted by CFS, the effect of CFS retrofitting on structural performance of the wall was examined continuously. Furthermore, the evaluation method of deformation performance of specimens was considered based on the test results.

2. Outline of Loading Test

2.1 Specimens

Figs.1 and 2 show the bar arrangement and schematic diagram of test specimens and Table 1 provides the test specimens list. There are a total of three specimens of RC structural walls without boundary columns. The test

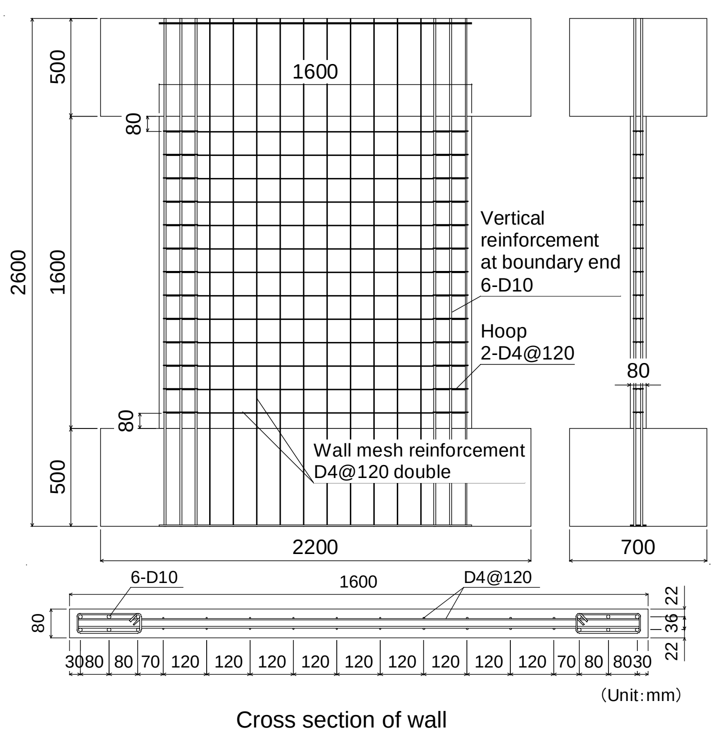

Fig. 1 – Bar arrangement (common to all test spesimens)

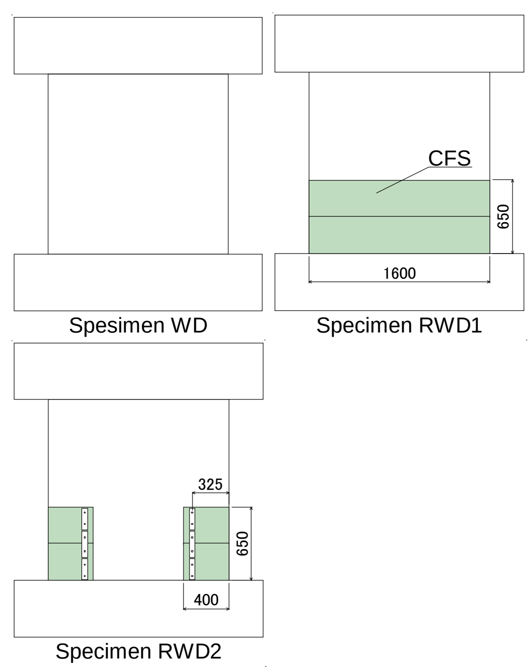

Fig. 2 – Schematic diagram of the test specimens

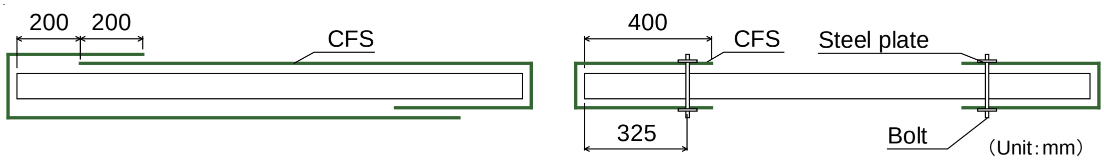

Fig. 3 – Attach CFS

Table 1 − Test specimens list

Specimen	WD	RWD1	RWD2
$l_w \times h_w$ (mm)	1600×1600		
Wall thickness t_w (mm)	80		
Vertical reinforcement at boundary ends	6-D10		
Hoop at boundary ends	D4@120		
Wall mesh reinforcement	D4@120 double (p_w=0.29%)		
Retrofit mode	Unretrofitted	Over wall span L=1600mm	Both boundary ends of wall, L=400mm/side

Table 2 – Concrete material properties

Specimen	σ_B (N/mm^2)	E_c (N/mm^2)	ε_{c0} (N/mm^2)	f_t (N/mm^2)	Age (days)
WD	26.7	23700	2200	2.7	37
RWD1	26.5	23000	2250	2.5	42
RWD2	28.3	23800	2500	3.0	53

σ_B: Compressisve srtrength, E_c : Modulus of elastisity, ε_{c0}: Strein at compressive at compressive strength, f_t: Tensile sterength by splite cylinder

Table 4 – CFS material properties

Fiber weight	g/m^3	300
Sheet thickness	Mm	0.167
Density	g/m^3	1.80
Tensile strength	kN/mm^2	3.4
Modulus of elasticity	kN/mm^2	230
Width	mm	330

Table 3 – Reinforcing steel material properties

Name (Property)	σ_y (N/mm^2)	E_s (N/mm^2)	σ_u (N/mm^2)	Use
D4	365	186000	524	Wall mesh reinforcement, Hoop at boundary ends
D10	371	182000	508	Vertical reinforcement at boundary ends

σ_y: Yield strength, E_s: Modulus of elasticity, σ_u: Tensile strength

valuables selected were the presence/absence of CFS retrofitting and the extent of retrofitting. Note that all three specimens were walls designed for flexural failure. The specimens were scaled to two-third, wall height was 1600 mm, wall length was 1600 mm, and wall thickness was 80 mm. Vertical reinforcement at boundary end was 6-D10, hoops at boundary end was D4@120, and wall mesh reinforcement was D4@120 double (p_w=0.29%) . The bar arrangement of these specimens were different from that of specimens in previous test. Previous specimens had single layer wall mesh reinforcement and vertical reinforcement at boundary ends, and don’t have hoop at boundary end.

Specimen WD represents the non-retrofitted test specimen for understanding the basic behavior of the walls. Specimen RWD1 was retrofitted over the entire wall span in height of 650mm at the bottom while specimen RWD2 was partially retrofitted at the boundary ends of the wall in height of 650mm at the bottom as shown in Fig. 2.

To attach the CFS, the corners of the walls were chamfered to a diameter of 13mm, epoxy resin was first applied to the wall surface, the CFS was then attached while maintaining tension manually and with a roller, and then epoxy resin was further applied on top with a roller to impregnate the CFS. Moreover, the top and bottom sheets were overlapped by 10 mm each. For specimen RWD2, the CFS was fixed by steel plates (PL-4.5) and threaded bolts (M10) as shown in Fig.3. And threaded bolts were tightened without management of tightening torque of bolts.

Tables 2 through 4 provide the concrete, reinforcing bars and CFS material properties. Used concrete was ordinary concrete of design strength of 24N/mm^2.

2.2 Loading program

A description of the loading device is presented in Fig. 4. A horizontal lateral force applied in cycles over the positive and negative directions was used for the loading. Also, a constant axial load (N = 0.08 l_w t_w F_c) of 273 kN was applied at the top of the specimen using a couple of vertical hydraulic jacks. Where, used F_c of compressive strength of concrete was 26.7 N/mm^2 in this calculation.

Additional moment was applied at the top of the specimen by controlling these vertical jacks to correspond to the acting shear force, such that the shear span ratio was 1.5, using the following equations.

$$N_e = \frac{N}{2} - \frac{Q}{l}(h_s - a), \quad N_w = \frac{N}{2} + \frac{Q}{l}(h_s - a) \tag{1}$$

Where, N_e: axial force of east side jack, N_w: axial force of west side jack, N: constant axial force, Q: lateral load, l: distance between two vertical jacks, h_s: assumed height of applied lateral load, and a: actual height of applied lateral load.

In the experiment, the horizontal displacement δ measured at the top stub, divided by the height of the measurement point h (1985 mm), was controlled through the drift angle of the member $R = \delta / h$. The loading cycle started with one cycle of R = 1/800 rad, and then two cycles each of R = 1/400, 1/200, 1/133, 1/100, 1/67, 1/50 and 1/33 rad.

2.3 Measuring method

In the tests, the horizontal displacement was measured, along with the longitudinal deformation at the boundary end of wall and partial deformation of the wall panel. The strains on the longitudinal, horizontal bars of the wall and CFS were measured using strain gages. Additionally, the widths of cracks were measured using a crack scale at each loading cycle.

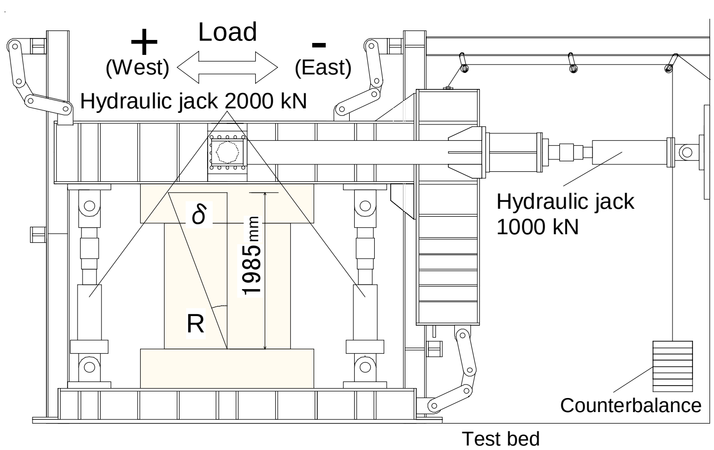

Fig. 4 – Description of loading apparatus

3. Test Results

3.1 Failure behavior and the relationship between lateral load and drift angle

The relationship between lateral load and drift angle for each specimen is given in Fig. 5. Also, Fig. 6 shows the condition at failure at the wall base for each specimen.

For specimen WD, flexural crack and flexural shear cracks appeared at the same cycle that the vertical wall reinforcement yielded under the R = 1/800 rad cycle, while the vertical reinforcement at boundary ends yielded under the R = 1/400 rad cycle. Afterwards, maximum capacity was reached at the R = 1/133 rad cycle. Concrete spalling at the lower part of the wall occurred under the second R = 1/100 rad cycle. Compression failure of concrete at the lower part of the wall occurred together with steep capacity deterioration under the R = 1/67 rad cycle, and buckling of vertical reinforcement at the boundary end was observed (Fig. 6(a)).

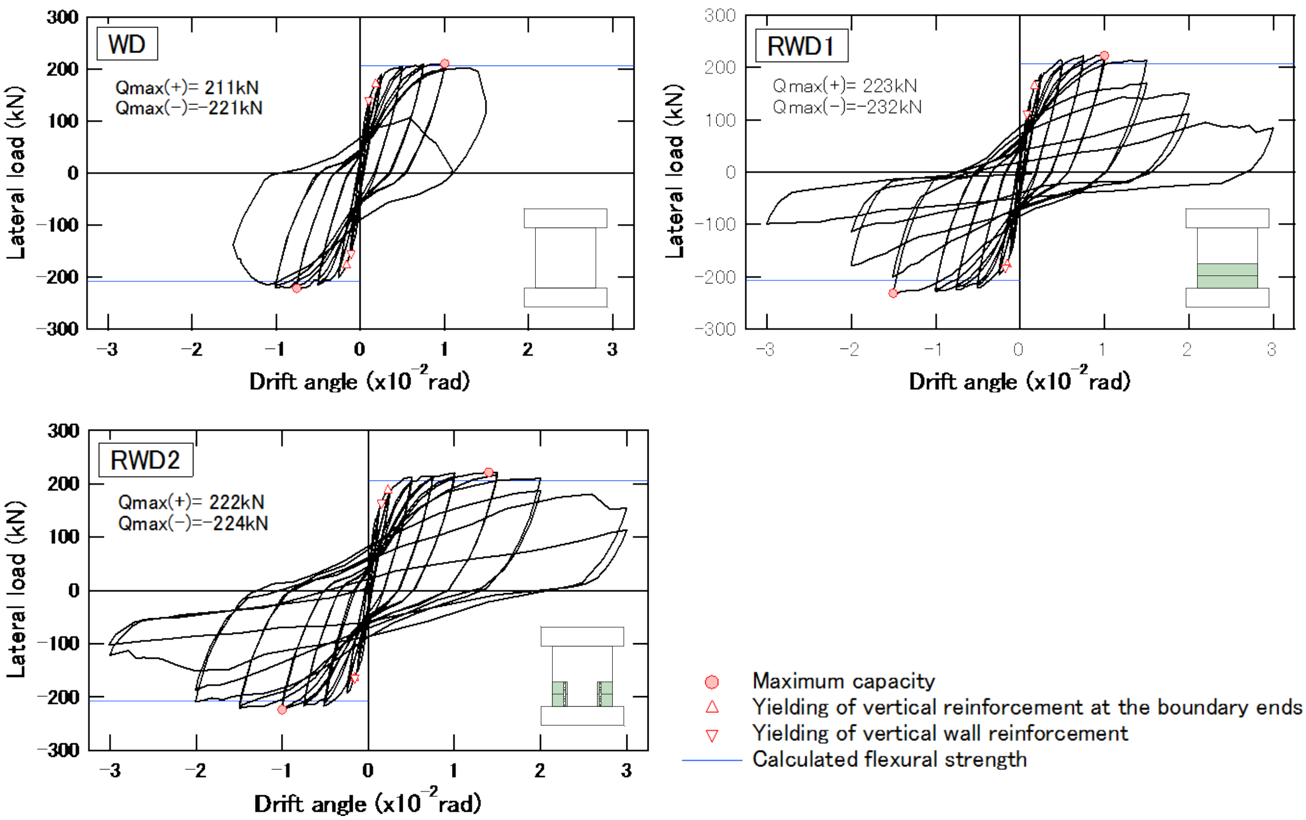

Fig. 5 – Lateral load and drift angle relationship

(a) WD (R=1/67 rad) (b) RWD1 (R=1/50 rad) (c) RWD2 (R=1/50 rad)

Fig. 6 – Wall base condition at failure for each specimen

For specimen RWD1, flexural crack and flexural shear cracks appeared at the same cycle that the vertical wall reinforcement yielded under the R = 1/800 rad cycle, while the vertical reinforcement at boundary ends yielded under the R = 1/400 rad cycle, similar to specimen WD. Maximum capacity was reached at the R = 1/67 rad cycle, the boundary end wrapped CFS began to swell. In subsequent loading cycles, concrete swelling at the wall base grew (Fig. 6(b)) until swelling occurred at the center of the lower part of the wall as well with capacity deterioration. Fracture of CFS occurred under the R =1/33 rad cycle.

For specimen RWD2, flexural crack and flexural shear cracks appeared under the R = 1/800 rad cycle, and the vertical wall reinforcement and the vertical reinforcement at boundary ends yielded under the R = 1/400 rad cycle. Maximum capacity was reached at the R = 1/100 rad cycle. The boundary end wrapped CFS began to swell at the same cycle, afterwards, concrete swelling at the wall base grew and capacity decreased with progress of loading cycle (Fig. 6(c)). Fracture of CFS occurred under the R =1/33 rad cycle.

3.2 Curvature distribution and deformation component

The curvature distribution during the first-cycle peak of each cycle is presented in Fig. 7. As shown in Fig. 8, the wall was divided into 4 sections over its height and the amount of displacements measured at each section. From these displacements, the average curvature was obtained for each section assuming a planar surface was kept. In each specimen, an increasing trend for the wall base curvature could be seen as the loading progressed. And the curvature concentrated at the wall base in the loading cycle of steep capacity deterioration. In particular, it was found that the most curvature of specimen RWD1 retrofitted over the entire wall span occurred at the wall base.

Fig. 9 shows the ratio of flexural to shear deformation at the time of positive peak loading. The flexural deformation was then calculated as the sum of these lateral deformations of curvature of Fig. 7. The shear deformation was calculated as the lateral displacement minus the flexural deformation. For all specimens, flexural deformation maintained a ratio of about 80% of the total, accounting for much of the overall deformation. And it was found that the flexural deformation increased in loading cycle that compression failure of concrete at the boundary end of wall base.

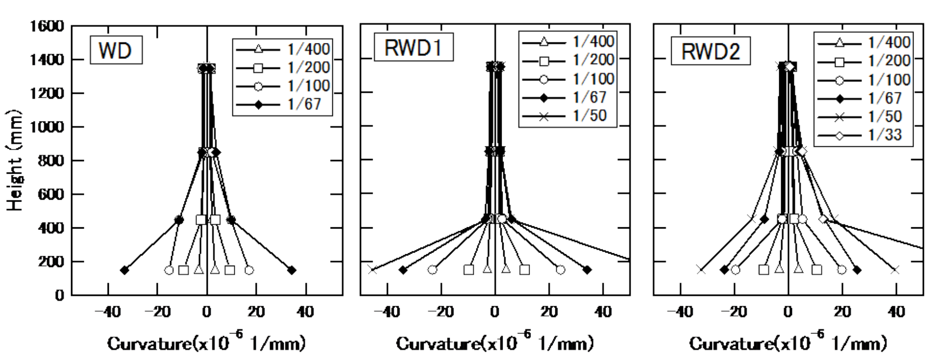

Fig.7 – Curvature distribution

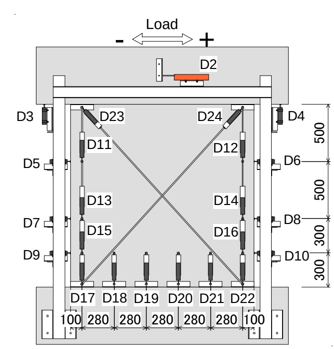

Fig.8 – Displacement gauge measurement points

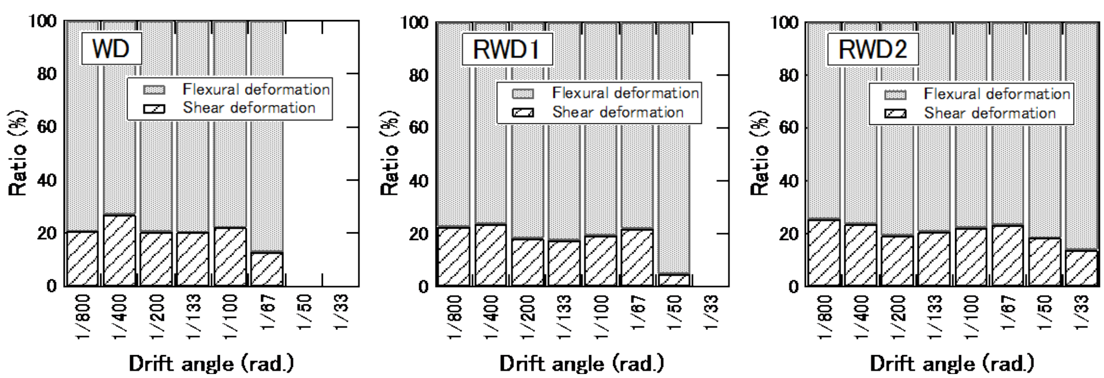

Fig.9 – Ratio of flexural to shear deformation

3.3 Deformation distribution at the wall base

Fig. 10 shows the wall base deformation distribution at the positive peak loading (displacements D17 - D22 in Fig. 8). For all the specimens, an increasing trend for the wall base deformation could be seen as the loading progressed. The displacements were found to be linearly distributed for all the specimens, confirming that the wall maintained a planar surface until loading cycle with capacity deterioration. Furthermore, for specimens RWD1 and RWD2, displacements at the compressive end were larger than that of specimen WD.

3.4 Ultimate flexural deformation

Fig. 11 shows the envelope curve of relationship between lateral load and flexural deformation, and ultimate flexural deformation for each specimen. The ultimate flexural deformation was obtained as the flexural deformation when lateral force decrease at 80 percent of maximum capacity. As ultimate deformation of specimen RWD1 was not on the envelop curve, ultimate deformation of specimen RWD1 was calculated with linear interpolation between peak of loading cycles as shown in fig. 11.

Maximum capacity for each specimen were the almost same, the capacity of specimen RWD1 and specimen RWD2 which were retrofitted by CFS showed more gradual deterioration than that of non-retrofitted specimen WD. As results, it was found that the ultimate flexural deformation of retrofitted specimens was increase and the deformation capacity improved.

Fig. 12 shows vertical strain of concrete at the compressive end of wall base. The vertical strain was calculated with displacement measured transducer of D22 shown in Fig. 8. Note that minus in vertical axis indicates compressive direction in this figure.

It was found that the vertical strain at the compressive end of specimen WD was increase steeply near -0.01 of strain or ultimate deformation of the wall. As for retrofitted specimen, the vertical strains near ultimate

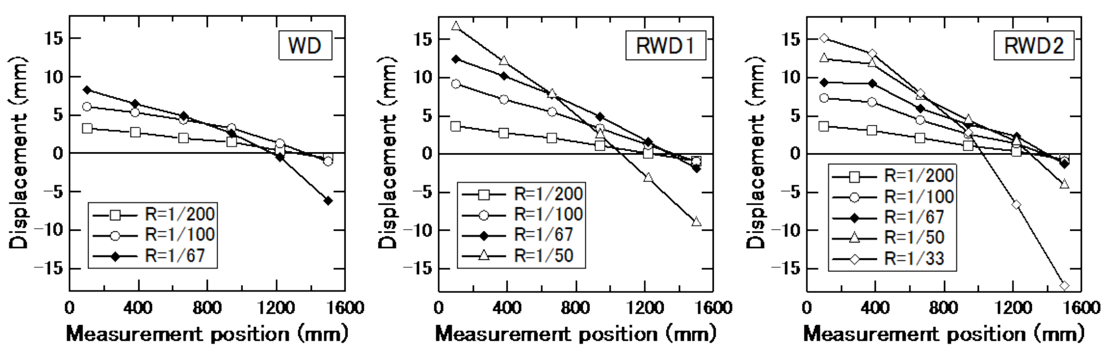

Fig.10 – Wall base deformation distribution

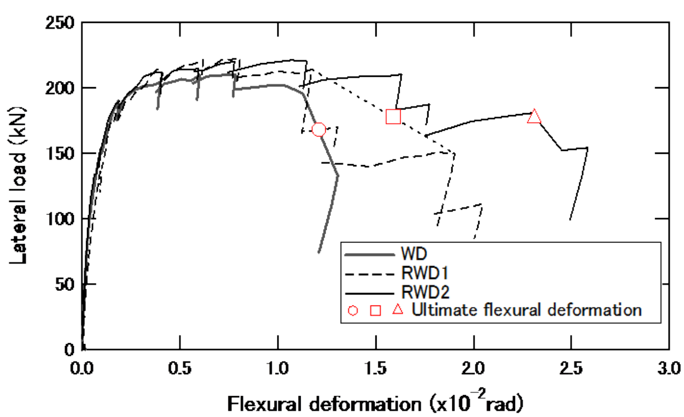

Fig.11 – Ultimate flexural deformation

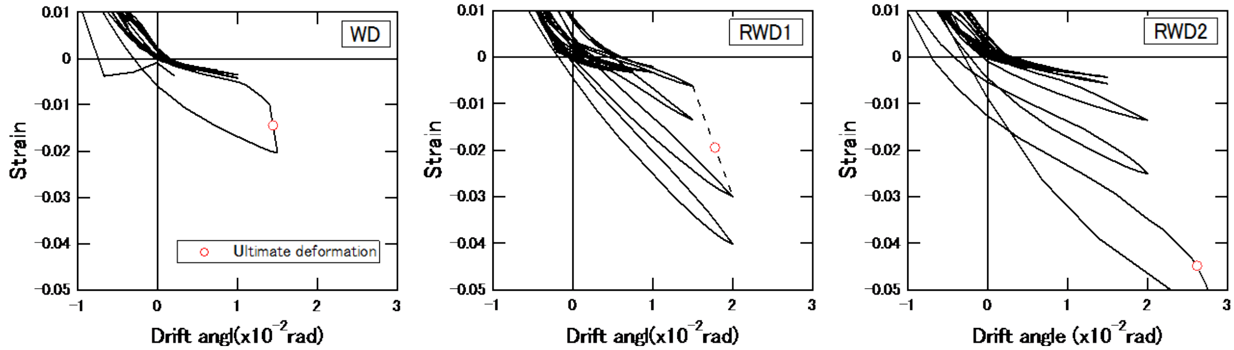

Fig.12 – Strain of concrete at the compressive end of wall base

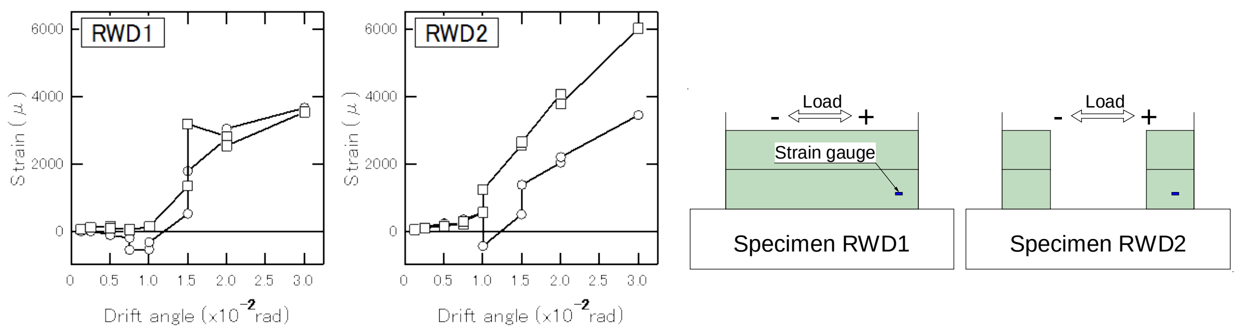

Fig.13 – CFS Strainat the boundary end of wall base

deformation of specimen RWD1 and specimen RWD2 were about -0.03 and -0.04 respectively, these were larger than that of specimen WD. It was thought that concrete retrofitted by CFS could contribute for compression stress in even larger strain region than non-retrofitted concrete due to constraining concrete by CFS.

3.5 CFS strain

Fig. 13 indicates the CFS strain in fiber direction for specimens RWD1 and RWD2. The strains were measured at the both side of wall at the locations of the strain gauges shown in Fig. 13. As for Specimen RWD1, the CFS strain reached about 3000 μ around the ultimate deformation. While the CFS strain of specimen RWD2 reached 5000 μ around the ultimate deformation, the CFS strain of specimen RWD2 was larger than that of specimen RWD1. It was found that the CFS resisted swelling of concrete with the progress of compressive failure of concrete at the wall base.

4. Considerration of Ultimate flexural deformation

In this chapter, ultimate flexural deformation of specimens is examined, calculation method is considered as the following. The ultimate flexural deformation R_u is composed of elastic deformation R_y and plastic deformation R_p (Eq.(2)).

$$R_u = R_y + R_p \tag{2}$$

And curvature distribution is assumed to be as shown in Fig. 13 in the calculation, as the curvature concentrated at the wall end in the loading cycle of steep capacity deterioration as shown in Fig.7. The elastic component is given by Eq. (3) from assumed curvature distribution of trapezoidal, the curvature at the yielding ϕ_y is considered as curvature when strain at the center of vertical reinforcements at boundary ends reach yielding strain of the reinforcement ε_y.

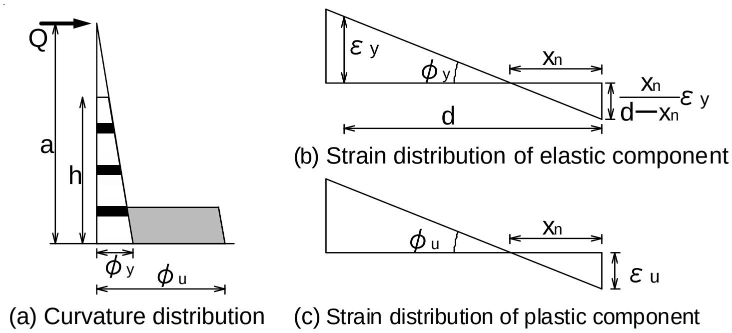

Fig.13 – Assumed carvature distribution and strain distribution

Table 4 – Test result at the ultimate flexural deformation

Specimen	Ultimate flexural deformation ($\times 10^{-2}$rad.)	ε_u	x_n (mm)
WD	1.21	–0.020	361
RWD1	1.59	–0.025	412
RWD2	2.31	–0.056	531

$$R_y = \left(\frac{h}{2} - \frac{h^2}{6a} \right) \phi_y \tag{3}$$

Where, a is shear span length, h is measurement point height of lateral displacement in the specimens. The plastic component of ultimate flexural deformation is calculated by Eq. (5) from Eqs. (2) and (4).

$$\phi_u = \frac{\varepsilon_u}{x_n} \tag{4}$$

$$R_p = L_p \left(\phi_u - \phi_y \right) = \frac{L_p}{x_n} \left(\varepsilon_u - \frac{x_n}{d - x_n} \varepsilon_y \right) \tag{5}$$

Where, ϕ_u is the ultimate curvature, ε_u is the ultimate compressive strain of concrete at the compression end, x_n is the neutral axis depth, L_p is the plastic hinge length.

It is important to appropriately evaluate the neutral axis depth x_n, the ultimate compressive strain of concrete ε_u, and the plastic hinge length L_p in order to evaluate ultimate flexural deformation based on above calculation method. Evaluation of x_n and ε_u relate a stress–strain curve of concrete retrofitted by CFS. Although some studies on constraining effect of CFS on stress-strain curve of concrete were conducted, study on rectangular cross-section concrete which have comparative large ratio of depth to width is few [4, 5]. Therefore, in this consideration, the ultimate flexural deformation is calculated by using test results of x_n and ε_u, the consistency between test and calculation result of the ultimate flexural deformation is examined as basic consideration.

Table 4 shows the test result at the ultimate flexural deformation. The neutral axis depth in the test x_n is obtained as the neutral axis depth at the ultimate deformation by vertical displacement at the wall base. The ultimate compressive strain of concrete at the compression end ε_u is calculated as the strain at the ultimate deformation in compression end from vertical displacement at the wall base, assuming the concrete uniformly deforms in plastic hinge zone. Two value of 200mm and 300mm of plastic hinge length L_p are used in calculation from the result that plastic hinge length is supposed be between 200mm to 300mm as shown in Fig. 6 (a), and Fig. 14.

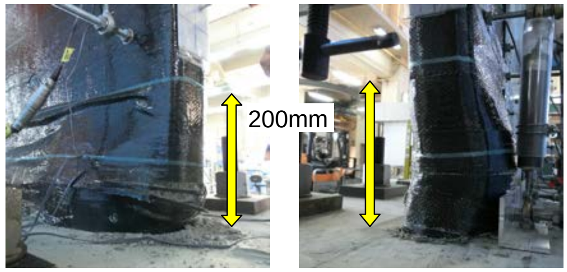

(a) RWD1 (R=1/33rad) (b) RWF2 (R=–1/50)

Fig. 14 – Damage of wall base

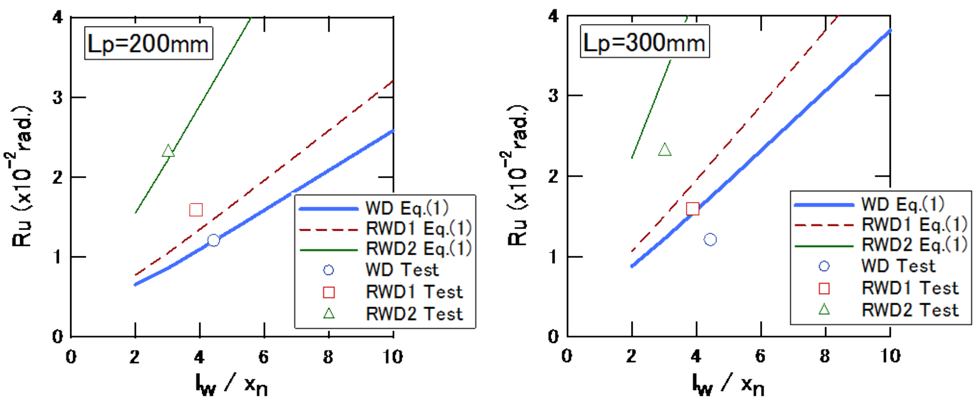

Fig – 15 Calculated and experimental ultimate flexural deformation

The calculated and experimental ultimate flexural deformation is shows in Fig. 15. The horizontal axis is l_w/x_n, where l_w is wall whole length. As for the result with 200mm of L_p, calculated ultimate flexural deformation is good agreement with experimental value. As for the result with 300mm of L_p, experimental results are smaller than calculated results. The calculated ultimate flexural deformation with 200mm (0.125 times length of whole length of wall, 2.5 times length of wall thickness) of L_p could be good agreement with the test results.

5. Conclusion

An experimental study was conducted on structural performance of rectangular RC shear walls retrofitted by carbon fiber sheets, and calculation method of the ultimate flexural deformation was examined. The following findings were obtained.

By retrofitting the RC shear wall without boundary columns with CFS, post-maximum strength deterioration was more gradual, confirming the improvement in deformation performance.

Ultimate flexural deformation of specimen which was partially retrofitted at the boundary ends of wall was larger than that of specimen which was retrofitted over the entire wall span.

Vertical strain of concrete in compression end at the wall base of retrofitted specimens was larger than that of non-retrofitted specimen around ultimate deformation. Thus, it was expected that concrete of shear wall retrofitted by carbon fiber sheets would be resistant to lager compressive force than that of non-retrofitted shear wall in even large strain region.

In the case of evaluation with 200mm of plastic hinge length L_p, calculated ultimate flexural deformation was good agreement with the experimental result.

In the future, it is necessary to understand compression characteristics of confined concrete by CFS and examine about evaluation of neutral axis depth x_n and ultimate compressive strain of concrete ε_u used in calculation of ultimate flexural deformation of the retrofitted walls.

Acknowledgements

This study was conducted with a grant from the "Enhancement of Earthquake and Tsunami Disaster Mitigation Technology in Peru" (Principal Investigator: Prof. Fumio Yamazaki, Chiba University), a project of the Science and Technology Research Partnership for Sustainable Development (SATREPS) program, a collaboration of JST (Japan Science and Technology Agency) and JICA (Japan International Cooperation Agency). Also, the authors would like to acknowledge the contribution of Toray Industries, Inc., by providing materials and technical guidance during the making of the retrofit specimens. We take this opportunity to express our appreciation.

References

[1] Architectural Institute of Japan (2012): *Reconnaissance Report of the 2010 Chile Off Maule Earthquake*

[2] T. Matsui, T. Saito and R. Ericksen (2014): Basic Study on Reinforced Concrete Shear Walls Without Boundary Columns Retrofitted by Carbon Fiber Sheets, *Journal of Disaster Research*, Vol.9, No.6, 1008-1014

[3] K. Horie, Y. Matsuzaki, H. Fukuyama, M. Iso, N. Yoshida, and N. Hayashida (1997): A Study on Retrofitting of Shear Wall with Continuous Fiber Sheet, *Summaries of technical papers of the Annual Meeting, Architectural Institute of Japan*, 595-600 (in Japanese)

[4] L. Lam and J.-G. Teng (2003) : Design-oriented Stress-Strain Model for FRP-confined Concrete in Rectangular Columns, *Journal of Reinforced Plastic and Composite*, Vol. 22, No. 13, 1149-1186

[5] K.A. Harries and S. A. Carey (2003) : Shape and “gap” effects on behavior of variably confined concrete, Cement and Concrete Research, 33, 881-890